ACS OMEGA

Open Access

http://pubs.acs.org/journal/acsodf

Article

Enhanced Energy Density in All-in-One Device Integrating Si Solar Cell and Supercapacitor Using [BMIm]Cl/PVA Gel Electrolyte

Chung Lee, Iyan Subiyanto, Segi Byun, Seong Ok Han, Churl-Hee Cho,* and Hyunuk Kim*

Cite This: *ACS Omega* 2024, 9, 7255−7261

Read Online

ACCESS | Metrics & More | Article Recommendations | Supporting Information

ABSTRACT: All-in-one systems integrating solar cells and supercapacitors have recently received significant attention because of their high efficiency and portability. Unlike conventional solar photovoltaics, which require external wiring to connect to a battery for energy storage, integrated devices with solar cells and supercapacitors share one electrode, eliminating wiring resistance and facilitating charge transfer. In this work, we designed and fabricated all-in-one devices by combining a silicon solar cell and a supercapacitor with polymer gel electrolytes. Our all-in-one devices incorporating H_3PO_4/PVA and [BMIm]Cl/PVA exhibited areal capacitances of 452.5 and 550 mF·cm $^{-2}$ at 0.1 mA·cm^{-2}, respectively, following 100 s of photocharging. Notably, the [BMIm]Cl/PVA-based all-in-one device demonstrated significantly higher maximum energy density and power density compared to both the H_3PO_4/PVA-based all-in-one device and the values reported in literature. In addition, the cyclic photocharge/galvanostatic discharge process for the [BMIm]Cl/PVA-based all-in-one device represented consistent retention of areal capacitance, affirming its stability across charge−discharge cycles. After 100 s of photocharging, the [BMIm]Cl/PVA-based all-in-one device achieved a total energy efficiency of 1.85%, surpassing the 1.45% efficiency observed in the device using H_3PO_4/PVA. These results provide valuable insights for the design of self-charging all-in-one devices for portable and wearable applications.

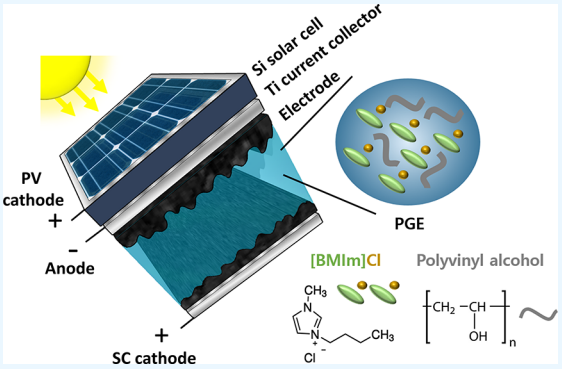

1. INTRODUCTION

Efficient energy storage generated by solar photovoltaics (PV) is critical for compact and portable electronic devices in the solar cell market.[1−6] To date, solar panels must be connected to batteries via external cables to store the energy, which reduces storage efficiency due to the long external circuit.[1] Furthermore, PV often faces significant uncertain intraday fluctuations, requiring fast charging of energy-storage devices. Integrating PV and a fast-charging device into a single unit can optimize energy efficiency through self-charging, cell volume, and flexibility, thereby opening up new markets for portable and wearable devices.[7−17] There are various all-in-one devices that integrate PV and energy storage.[2] In the case of an all-in-one device combining an N-type solar cell with an energy-storage component, the P−N junction enables electrons to move toward the n-type semiconductor when exposed to light, generating electron−hole pairs and establishing the n-type semiconductor as the anode of the battery. Simultaneously, the P-type semiconductor functions as the cathode, with holes (+) moving in the opposite direction, as depicted in Figure 1a. This configuration enables the rapid charging of energy-storage devices.

The integration of a PV device with energy storage faces challenges in efficiency and stability, prompting a focused effort among researchers to address these issues. In the initial stages, all-in-one devices combined silicon PV with supercapacitors, exhibiting storage capacity and conversion efficiency below 2%.[18,19] Despite this initial limitation, these early devices showed the potential for future enhancements. Notably, integration of a perovskite solar cell with lithium-ion batteries has demonstrated increased energy density. For instance, the incorporation of perovskite solar cells involved stacking four $CH_3NH_3PbI_3$ layers in series for direct photocharging of lithium-ion batteries assembled with a $LiFePO_4$ cathode and a $Li_4Ti_5O_{12}$ anode, achieving an overall photoelectric conversion and storage efficiency of 7.8% along with exceptional cycling stability.[20] Additionally, combining perovskite solar cells with lithium-ion batteries using a $Li_4Ti_5O_{12}$ anode and a $LiCoO_2$ cathode achieved an overall efficiency of 9.36% supported by a DC-DC voltage boost converter.[21]

Supercapacitors function as fast-charging energy-storage devices by utilizing the electrical double layer on electrode surfaces, storing energy through electrolyte physical adsorption

Received: December 8, 2023
Revised: January 16, 2024
Accepted: January 19, 2024
Published: February 1, 2024

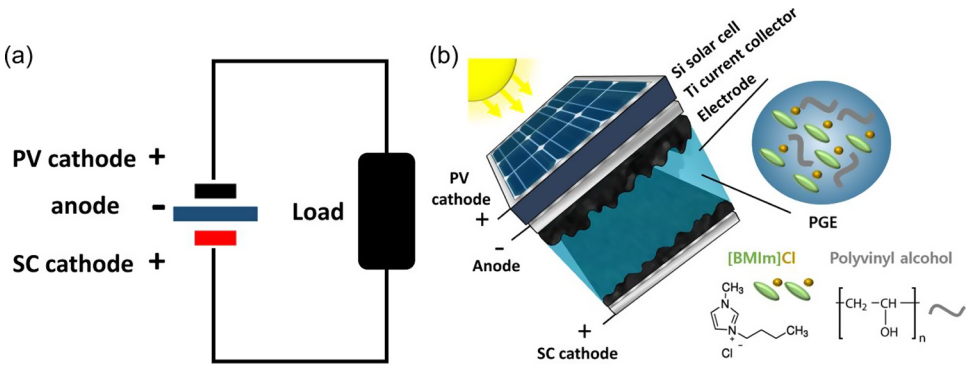

Figure 1. (a) Scheme of an integrated device combining PV and supercapacitor and (b) design of the all-in-one device in the work.

and exhibiting extended cycle life and rapid charging times.[22,23] However, challenges persist in integrating solar cells with rapid-charging supercapacitors, primarily concerning their relatively low energy density.[14] Overcoming this, challenge necessitates advancements in electrolytes due to the low ionic conductivity of current electrolytes, which limits the capacity of supercapacitors and consequently their energy density. Furthermore, conventional electrolytes often degrade under harsh conditions. To address these challenges, our study focuses on enhancing the electrochemical performance and thermal stability by employing polymer gel electrolytes (PGEs). PGEs offer low vapor pressure, high ionic conductivity, and broad working potential window, making them well-suited for efficient energy conversion and storage.[24] To prevent the risks associated with liquid electrolyte leakage, we synthesized quasi-solid electrolytes through gelation, combining poly(vinyl alcohol) (PVA) with proton-conducting H_3PO_4 and the aprotic ionic liquid 1-*n*-butyl-3-methylimidazolium chloride [BMIm]Cl.[25] This PVA matrix serves as the foundation of the electrolyte. A schematic representation of the integrated device is illustrated in Figure 1. Our all-in-one devices, incorporating H_3PO_4/PVA and [BMIm]Cl/PVA, exhibited areal capacitances of 452.5 and 550 mF·cm^{-2} at 0.1 mA·cm^{-2}, respectively, following 100 s of photocharging. In particular, the [BMIm]Cl/PVA-based all-in-one device demonstrated notably higher maximum energy density and power density in comparison with the H_3PO_4/PVA-based all-in-one device. Therefore, this suggests the suitability of the aprotic ionic liquid as an electrolyte for the integrated device. Significantly, the [BMIm]Cl/PVA-based all-in-one device exhibited substantial enhancements in energy density and a sustained cycle life when contrasted with values reported in the existing literature. The cyclic photocharge/galvanostatic discharge process for the [BMIm]Cl/PVA-based all-in-one device demonstrated consistent retention of areal capacitance, thus confirming its stability throughout charge−discharge cycles.

2. EXPERIMENTAL SECTION

2.1. Fabrication of All-in-One Device. The n-type slide of the solar cell (1.5 × 1.5 cm^2) was sputtered with Ti metal (approximately 100 nm thickness) to serve as the anode current collector. A Ti metal plate (1.5 × 1.5 cm^2) with a thickness of 1.5 mm was used as the cathode current collector. As depicted in Figure 1b, three electrodes (p-type slide, n-type Ti anode, and Ti plate cathode) were connected by a Cu wire and bonded with Ag paste as an adhesive. The assembly was then dried at 55 °C for 2 h. Both Ti current collectors were coated with the electrode slurry (comprising YP50-F active material:super-P conductive material:PVDF binder in a ratio of 80:10:10). Subsequently, they were dried at 70 °C for 4 h and then subjected to vacuum drying at 110 °C for 4 h. To prepare the gel electrolyte with [BMIM]Cl/PVA, a mixture of 0.921 g of [BMIM]Cl and 1.0 g of PVA was added to 10 mL of deionized water, and the mixture was stirred at 85 °C for 1 h. A glass microfiber separator (1.5 × 1.5 cm^2) was immersed in the [BMIM]Cl/PVA gel electrolyte solution for 24 h, facilitating the impregnation of the separator with the gel electrolyte.[26] For comparison, we prepared an alternative gel electrolyte using H_3PO_4/PVA. To achieve this, 5.0 g of H_3PO_4 and 5.0 g of PVA were added to 50 mL of deionized water and stirred at 85 °C for 1 h. Subsequently, a glass microfiber separator (1.5 × 1.5 cm^2) was immersed in the H_3PO_4/PVA gel electrolyte for 24 h to prepare the separator impregnated with the gel electrolyte. Then, as shown in Figure 1b, we assembled the electrodes and the separator to fabricate an all-in-one device integrating a solar cell and a supercapacitor (Figure S1). To prevent electrolyte leakage, we completely sealed the cell periphery with the ethylene vinyl acetate adhesive.

2.2. Electrochemical Analysis. Cyclic voltammetry (CV), galvanostatic charge−discharge (GCD), and current voltage (*IV*) studies were conducted by using a BioLogic VSP potentiostat and EC-Lab software within the specified voltage range. Photocharging experiments were performed under AM 1.5G 1 sun illumination using a solar simulator (QTH Light Source; Oriel Instruments). The AM 1.5G spectrum was calibrated and normalized to 1 kW/m^2. The specific capacitances of the electrodes (C_s, mF·cm^{-2}) were calculated from the discharge curves using eq 1 excluding the effects of the Ohmic drop. To assess the long-term stability, areal capacitance was measured over the course of 1 week. Ten measurements of areal capacitance were taken to establish the average values (Figure 4b). The energy density (E, W h·cm^{-2}) and power density (P, W·cm^{-2}) were calculated using eqs 2 and 3, respectively.[3] Here, I (A) is the constant current, Δt (s) is the discharge time, ΔV (V) represents the absolute discharge potential window, A (cm^2) corresponds to the electrode area, and C_s (mF·cm^{-2}) denotes the specific capacitance.

$$C_s = \frac{I\Delta t}{A\Delta V} \quad (1)$$

$$E = \frac{C\Delta V^2}{2} \quad (2)$$

https://doi.org/10.1021/acsomega.3c09812
ACS Omega 2024, 9, 7255−7261

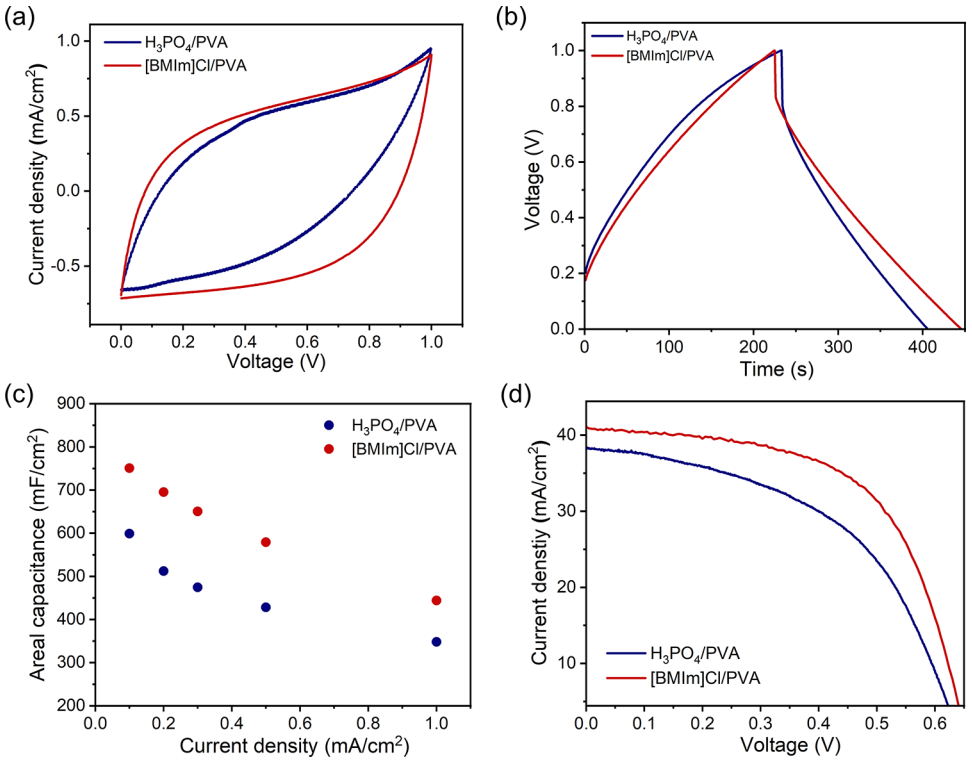

Figure 2. Electrochemical properties of the all-in-one devices: (a) CV curves at a scan of 3.0 mV/s, (b) GCD curves taken at a current density of 1.0 mA·cm^{-2}, (c) areal capacitances on discharge current densities, and (d) *IV*-curve at 5.0 mV·s^{-1}.

$$P = \frac{E}{\Delta t} \tag{3}$$

The power conversion efficiency (PCE) was calculated by using eq 4, where V_{OC} represents the open-circuit voltage, I_{SC} stands for the short-circuit current, and FF denotes the fill factor of the solar cell. The value of P_{in} corresponds to the solar radiation power (100 mW·cm^{-2} for 1 sun).

$$\text{PCE} = \frac{I_{sc} \times V_{oc} \times \text{FF}}{P_{in}} \tag{4}$$

The total conversion efficiency (η_{total}) of the integrated device was calculated using eq 5. In this equation, E_{in} (W h) stands for the total input energy obtained from light, P_{in} denotes the illuminated light density (100 mW·cm^{-2}), $t_{discharing}$ (h) represents the discharge time, and A (cm^2) corresponds to the electrode area.

$$\eta_{total} = \frac{E_{in}}{P_{in} \cdot A \cdot t_{discharging}} \tag{5}$$

3. RESULTS AND DISCUSSION

An integrated all-in-one device was developed by combining an n-type silicon solar cell with a supercapacitor. To fabricate a shared anode for both components, a 100 nm-thick titanium thin film was deposited onto the rear surface of the n-type Si solar cell. YP50-F activated carbon was uniformly coated on both Ti current collectors, resulting in the formation of symmetrical electrodes. To enhance the electrochemical performance and stability, polymer gel electrolytes of H_3PO_4/PVA and [BMIm]Cl/PVA were utilized. The electrochemical performance of the all-in-one devices was investigated by CV and GCD analyses (Figures S2 and S3). CV curves of the all-in-one devices were compared by measuring at a scan rate of 3.0 mV·s^{-1} in the voltage range from 0 to 1.0 V (Figure 2a). The CV profiles obtained for both devices showed a rectangle-like shape similar to that observed in electric double-layer capacitors (EDLCs), suggesting the physical adhesion of electrolytes to the activated carbon surface.[3] With increasing scan rates, higher current values were obtained. The GCD curves of the all-in-one devices are depicted in Figure 2b. For these curves, the cutoff voltage was set at 1.0, and the charge and discharge times were measured at a current density of 1.0 mA·cm^{-2}. The GCD curves exhibit a symmetrical triangular shape, consistent with the characteristic behavior of EDLCs. This shape demonstrates electrochemical reversibility attributed to the efficient adsorption and desorption of activated carbon and electrolyte ions. In solid-state and gel electrolytes, the transition from charging to discharging often leads to an Ohmic drop.[27] As depicted in Figure 2b, both H_3PO_4/PVA and [BMIm]Cl/PVA-based all-in-one devices display noticeable Ohmic drops. A closer analysis of the GCD curves highlights a slightly lower voltage drop in the [BMIm]Cl/PVA-based device compared to the H_3PO_4/PVA-based device. This characteristic extends the discharging time, consequently enhancing the discharge capacity. As the current density increases, the discharge capacity decreases proportionally. The relationship between the areal discharge capacity and the current density is illustrated in Figure 2c. The discharge capacities for the all-in-one devices incorporating H_3PO_4/PVA and [BMIm]Cl/PVA electrolytes are 599 and 750.8 mF·cm^{-2} at a current density of 0.1 mA·cm^{-2}, respectively. Notably, the all-in-one device with [BMIm]Cl/PVA demonstrated significantly higher areal capacitances than those with H_3PO_4/PVA across all current densities. IV curves were obtained for the all-in-one devices under simulated AM 1.5G 1 sun illumination, as

https://doi.org/10.1021/acsomega.3c09812
ACS Omega 2024, 9, 7255−7261

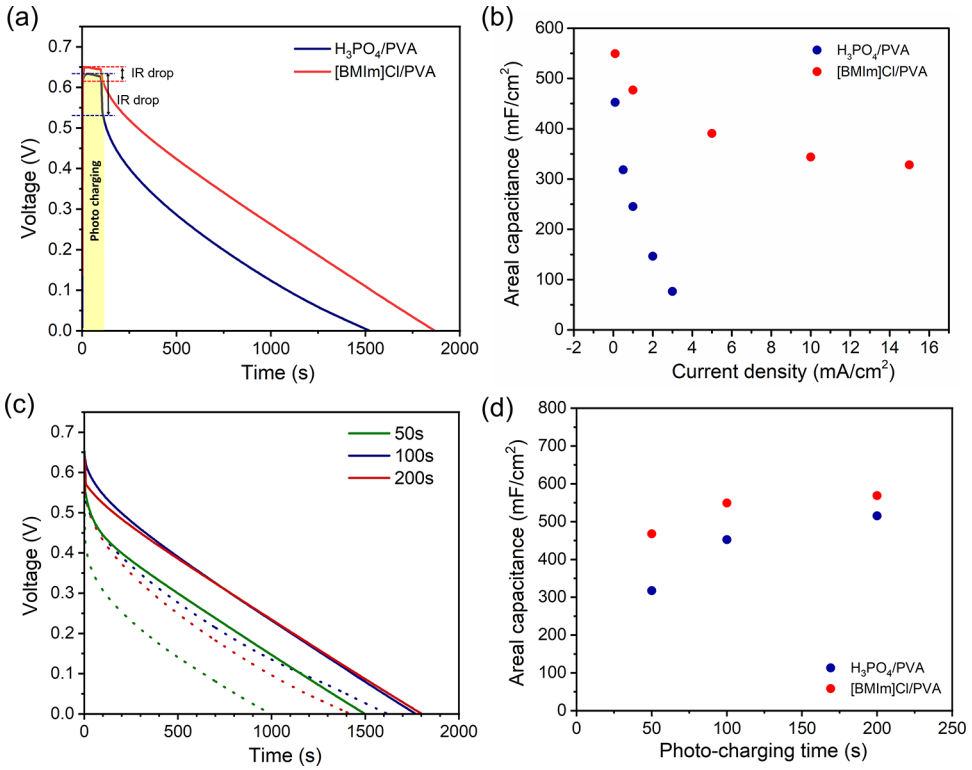

Figure 3. Photocharging and galvanostatic discharging properties of all-in-one devices: (a) discharge curves at 0.1 mA·cm^{-2} after a photocharging time of 100 s (IR drop for H_3PO_4/PVA and [BMIm]Cl/PVA device: 0.1 and 0.04 V, respectively), (b) areal capacities at different current densities, (c) discharge curves of H_3PO_4/PVA (dotted line) and [BMIm]Cl/PVA-based (solid line) all-in-one devices after 50 s (green), 100 s (blue), and 200 s (red) of photocharging, and (d) areal capacitance at various photocharging times of 50, 100, and 200 s under 1 sun illumination.

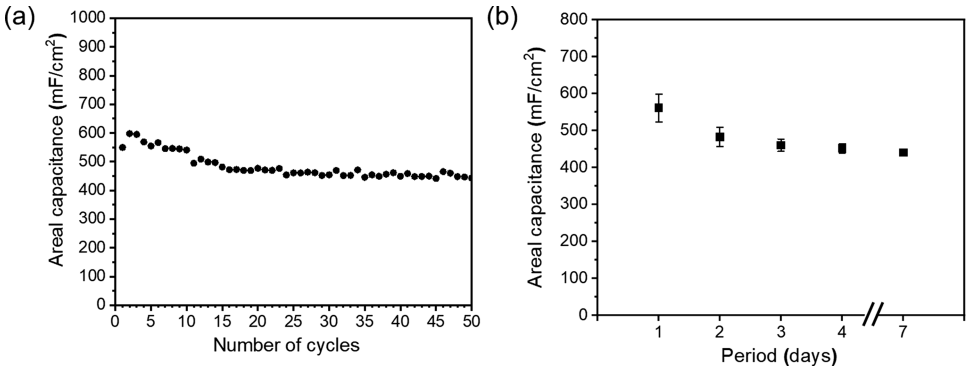

Figure 4. (a) Areal capacitance cycles of the [BMIm]Cl/PVA-based all-in-one device at 0.1 mA·cm^{-2} following a 100 s photocharging time and (b) average areal capacitance after the period (areal capacitance was measured 10 times).

depicted in Figure 2d. When considering the ratio of the maximum power (P_{max}) to the input power (P_{in}), the PCEs were calculated to be 12% for all-in-one devices with H_3PO_4/PVA and 13.0% for the one with [BMIm]Cl/PVA.

To investigate photocharging and galvanostatic discharging in H_3PO_4/PVA and [BMIm]Cl/PVA-based all-in-one devices, discharging curves were measured at various current densities following exposure to 1 sun illumination. H_3PO_4/PVA- and [BMIm]Cl/PVA-based all-in-one devices have linear discharge curves, which is characteristic of an electrical double-layer capacitor, proving that the incident light energy is converted and stored in the supercapacitor. The internal resistances, calculated from the voltage drop, for the H_3PO_4/PVA and [BMIm]Cl/PVA-based all-in-one devices are 64 and 27 Ω, respectively, representing a significant decrease compared to the literature values (Figure 3a).[28] At a current density of 0.1 mA·cm^{-2}, the areal discharge capacitance for H_3PO_4/PVA and [BMIm]Cl/PVA-based all-in-one devices reaches 452.5 and 550 mF·cm^{-2}, respectively (Figure 3a). The [BMIm]Cl/PVA-based all-in-one device exhibited significantly higher areal capacitances than the H_3PO_4/PVA-based all-in-one device across various current densities. This enhancement is attributed to a markedly lower IR drop in the [BMIm]Cl/PVA-based device (Figure 3a). To elucidate this disparity, the self-discharge measurement was conducted following photocharging (Figure S7). The self-discharge was monitored for 1 h after 100 s photocharging. While the H_3PO_4/PVA-based device exhibited rapid self-discharge, the [BMIm]Cl/PVA-based device sustained 0.43 V after 1 h of monitoring, indicating superior stability. As the current density increases,

https://doi.org/10.1021/acsomega.3c09812
ACS Omega 2024, 9, 7255−7261

the areal capacitance decreases (Figure 3b). To determine the optimal photocharging time, we measured the discharge curves for H_3PO_4/PVA and [BMIm]Cl/PVA-based all-in-one devices after photocharging for 50, 100, and 200 s under 1 sun illumination (Figure 3c). Figure 3d highlights that photocharging time of 100 s is sufficient to charge the all-in-one device.

To demonstrate the stability of cyclic photocharging and galvanostatic discharging for the [BMIm]Cl/PVA-based all-in-one device, consecutive experiments were performed. As shown in Figure 4a, the areal discharge capacity is 443 mF·cm^{-2} after 50 times charge−discharge cycling consecutively and reached 81% of the initial value of 550 mF·cm^{-2}. Furthermore, after 1 week, the average areal discharge capacity was still 443 mF·cm^{-2}, indicating the stable performance of the all-in-one device (Figure 4b). The H_3PO_4/PVA-based all-in-one device also showed stable cyclic photocharging and galvanostatic discharging (Figure S6). The Ragone plot in Figure 5 shows the energy density and power density

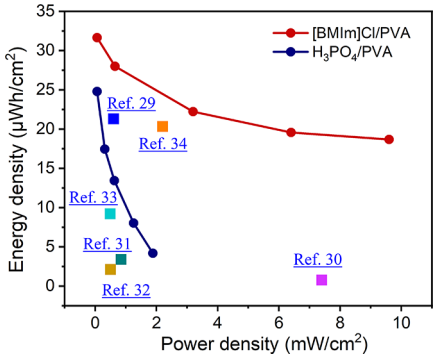

Figure 5. Ragone plot of integrated devices with supercapacitors.[29−34]

calculated at various discharge and charge and discharge rates. The maximum areal energy density of the [BMIm]Cl/PVA-based all-in-one device reached 31.65 μW h·cm^{-2}, which is significantly higher than those reported in the literature for other integrated devices with supercapacitors (Figure 5 and Table S1).[29−35] As the areal power density increased from 0.0644 to 9.6 mW·cm^{-2}, the areal energy density monotonically decreased from 31.65 to 18.67 μW h·cm^{-2}, which is characteristic for energy-storage devices.[36] The total energy efficiency of a photoelectrochemical capacitor was determined by dividing the stored energy in the supercapacitor by the total input energy from light, indicating the photoelectric conversion-to-storage efficiency. As listed in Table S2, the total energy efficiencies of all-in-one devices with H_3PO_4/PVA and [BMIm]Cl/PVA are 1.45 and 1.85% after a photocharging time of 100 s, which are comparable to other devices in the literature.

4. CONCLUSIONS

In conclusion, we have successfully fabricated an all-in-one device combining an N-type silicon solar cell and a supercapacitor, effectively addressing the challenge of efficient energy storage in photovoltaic systems. The device features a titanium thin film coated with activated carbon, serving as a shared anode for both the solar cell and supercapacitor components. The incorporation of polymer gel electrolytes, such as [BMIm]Cl/PVA or H_3PO_4/PVA, further enhances the electrochemical performance. With photocharging for 100 s, the H_3PO_4/PVA and [BMIm]Cl/PVA-based all-in-one devices exhibited an excellent areal capacitance of 452.5 and 550 mF·cm^{-2} at a current density of 0.1 mA·cm^{-2}, respectively. Notably, the [BMIm]Cl/PVA-based all-in-one device achieved a remarkable maximum energy density of 31.65 μW h·cm^{-2} and a maximum power density of 9.6 mW·cm^{-2}, both significantly surpassing values reported in the existing literature. Furthermore, the all-in-one device demonstrated exceptional cyclic stability, retaining 81% of its initial areal capacitance following 50 cycles and maintaining an average areal capacitance of 443 mF·cm^{-2} even after a week. Our results highlight the immense potential of integrating n-type solar cells and supercapacitors to lead high-performance all-in-one devices characterized by outstanding cyclic stability and remakable energy density. This achievement presents a promising avenue for advancing efficient solar energy conversion and storage technologies.

■ ASSOCIATED CONTENT

Data Availability Statement

The data underlying this study are not publicly available due to security reasons at our institute (KIER). The data are available from the corresponding author upon reasonable request.

Supporting Information

The Supporting Information is available free of charge at https://pubs.acs.org/doi/10.1021/acsomega.3c09812.

Images of all-in-one devices, CV and GCD curves at various current rates, photocharging and discharging curves, self-discharge curves (PDF)

■ AUTHOR INFORMATION

Corresponding Authors

Churl-Hee Cho − *Graduate School of Energy Science and Technology, Chungnam National University, Daejeon 34134, Republic of Korea*; Email: choch@cnu.ac.kr

Hyunuk Kim − *Hydrogen Convergence Materials Laboratory, Korea Institute of Energy Research, Daejeon 34129, Republic of Korea; Graduate School of Energy Science and Technology, Chungnam National University, Daejeon 34134, Republic of Korea; Energy Engineering, University of Science and Technology, Daejeon 34113, Republic of Korea*; orcid.org/0000-0002-2668-8267; Email: hyunuk@kier.re.kr

Authors

Chung Lee − *Hydrogen Convergence Materials Laboratory, Korea Institute of Energy Research, Daejeon 34129, Republic of Korea; Graduate School of Energy Science and Technology, Chungnam National University, Daejeon 34134, Republic of Korea*

Iyan Subiyanto − *Hydrogen Convergence Materials Laboratory, Korea Institute of Energy Research, Daejeon 34129, Republic of Korea; Energy Engineering, University of Science and Technology, Daejeon 34113, Republic of Korea*

Segi Byun − *Hydrogen Convergence Materials Laboratory, Korea Institute of Energy Research, Daejeon 34129, Republic of Korea*; orcid.org/0000-0001-6413-5658

Seong Ok Han − *Hydrogen Convergence Materials Laboratory, Korea Institute of Energy Research, Daejeon 34129, Republic of Korea*

Complete contact information is available at: https://pubs.acs.org/10.1021/acsomega.3c09812

https://doi.org/10.1021/acsomega.3c09812
ACS Omega 2024, 9, 7255−7261

Notes

The authors declare no competing financial interest.

■ ACKNOWLEDGMENTS

This study was conducted within the framework of the Research and Development Program of the Korea Institute of Energy Research (C4-2410&C4-8205-1). It was also supported by the Center for Advanced Meta-Materials (CAMM), which is funded by the Korean Ministry of Science and ICT (MSIT) as a Global Frontier Program (2019M3A6B3030636). This work was partially supported by Korea Environment Industry & Technology Institute (KEITI) through R&D project for Management of Atmosphere environment, funded by Korea Ministry of Enviornment (ME) (Grant Number: 2021003390008).

■ REFERENCES

(1) Lee, M. M.; Teuscher, J.; Miyasaka, T.; Murakami, T. N.; Snaith, H. J. Efficient hybrid solar cells based on meso-superstructured organometal halide perovskites. *Science* **2012**, *338* (6107), 643−647.
(2) Todorov, T. K.; Reuter, K. B.; Mitzi, D. B. High-Efficiency Solar Cell with Earth-Abundant Liquid-Processed Absorber. *Adv. Mater.* **2010**, *22*, E156−E159.
(3) O'Regan, B.; Grätzel, M. A Low-Cost, High-Efficiency Solar Cell Based on Dye-Sensitized Colloidal TiO_2 Films. *Nature* **1991**, *353*, 737−740.
(4) Rafique, A.; Ferreira, I.; Abbas, G.; Baptista, A. C. Recent Advances and Challenges Toward Application of Fibers and Textiles in Integrated Photovoltaic Energy Storage Devices. *Nano-Micro Lett.* **2023**, *15* (1), 40.
(5) Bandara, T. M. W. J.; Hansadi, J. M. C.; Bella, F. A Review of Textile Dye-Sensitized Solar Cells for Wearable *Electronics. Ionics* **2022**, *28* (6), 2563−2583.
(6) Dokouzis, A.; Bella, F.; Theodosiou, K.; Gerbaldi, C.; Leftheriotis, G. Photoelectrochromic Devices with Cobalt Redox Electrolytes. *Mater. Today Energy* **2020**, *15*, No. 100365.
(7) Vega-Garita, V.; Ramirez-Elizondo, L.; Narayan, N.; Bauer, P. Integrating a Photovoltaic Storage System in One Device: A Critical Review. *Prog. Photovolt. Res. Appl.* **2019**, *27*, 346−370.
(8) Gurung, A.; Qiao, Q. Solar Charging Batteries: Advances, Challenges, and Opportunities. *Joule* **2018**, *2*, 1217−1230.
(9) Zeng, Q.; Lai, Y.; Jiang, L.; Liu, F.; Hao, X.; Wang, L.; Green, M. A. Integrated Photorechargeable Energy Storage System: Next-Generation Power Source Driving the Future. *Adv. Energy Mater.* **2020**, *10*, No. 1903930.
(10) Lv, J.; Xie, J.; Mohamed, A. G. A.; Zhang, X.; Wang, Y. Photoelectrochemical Energy Storage Materials: Design Principles and Functional Devices Towards Direct Solar to Electrochemical Energy Storage. *Chem. Soc. Rev.* **2022**, *51*, 1511−1528.
(11) Namsheer, K.; Rout, C. S. Photo-Powered Integrated Supercapacitors: A Review on Recent Developments, Challenges and Future Perspectives. *J. Mater. Chem. A* **2021**, *9*, 8248−8278.
(12) Yun, S.; Qin, Y.; Uhl, A. R.; Vlachopoulos, N.; Yin, M.; Li, D.; Han, X.; Hagfeldt, A. New-Generation Integrated Devices Based on Dye-Sensitized and Perovskite Solar Cells. *Energy Environ. Sci.* **2018**, *11*, 476−526.
(13) Fagiolari, L.; Sampò, M.; Lamberti, A.; Amici, J.; Francia, C.; Bodoardo, S.; Bella, F. Integrated Energy Conversion and Storage Devices: Interfacing Solar Cells, Batteries, and Supercapacitors. *Energy Storage Mater.* **2022**, *51*, 400−434.
(14) Ng, C. H.; Lim, H. N.; Hayase, S.; Harrison, I.; Pandikumar, A.; Huang, N. M. Potential Active Materials for Photo-Supercapacitor: A Review. *J. Power Sources* **2015**, *296*, 169−185.
(15) Lau, D.; Song, N.; Hall, C.; Jiang, Y.; Lim, S.; Perez-Wurfl, I.; Ouyang, Z.; Lennon, A. Hybrid Solar Energy Harvesting and Storage Devices: The Promises and Challenges. *Mater. Today Energy* **2019**, *13*, 22−44.
(16) Tuc Altaf, C.; Rostas, A. M.; Popa, A.; Toloman, D.; Stefan, M.; Demirci Sankir, N.; Sankir, M. Recent Advances in Photochargeable Integrated and All-in-One Supercapacitor Devices. *ACS Omega* **2023**, *8*, 47393−47411.
(17) Yang, G.; Yang, W.; Gu, H.; Fu, Y.; Wang, B.; Cai, H.; Xia, J.; Zhang, N.; Liang, C.; Xing, G.; Yang, S.; Chen, Y.; Huang, W. Perovskite Solar Cell Powered Integrated Fuel Conversion and Energy Storage Devices. *Adv. Mater.* **2023**, *35*, No. 2300383.
(18) Westover, A. S.; Share, K.; Carter, R.; Cohn, A. P.; Oakes, L.; Pint, C. L. Direct Integration of a Supercapacitor into the Backside of a Silicon Photovoltaic Device. *Appl. Phys. Lett.* **2014**, *104* (21), 213905.
(19) Pirrone, N.; Bella, F.; Hernández, S. Solar H_2 Production Systems: Current Status and Prospective Applications. *Green Chem.* **2022**, *24* (14), 5379−5402.
(20) Xu, J.; Chen, Y.; Dai, L. Efficiently Photo-Charging Lithium-Ion Battery by Perovskite Solar Cell. *Nat. Commun.* **2015**, *6* (1), 8103.
(21) Gurung, A.; Chen, K.; Khan, R.; Abdulkarim, S. S.; Varnekar, G.; Pathak, R.; Naderi, R.; Qiao, Q. Highly Efficient Perovskite Solar Cell Photocharging of Lithium Ion Battery Using DC−DC Booster. *Adv. Energy Mater.* **2017**, *7* (11), No. 1602105.
(22) Sun, X.; Zhang, X.; Zhang, H.; Huang, B.; Ma, Y. Application of a Novel Binder for Activated Carbon-Based Electrical Double Layer Capacitors with Nonaqueous Electrolytes. *J. Solid State Electrochem.* **2013**, *17*, 2035−2042.
(23) Zhang, L. L.; Zhao, X. S. Carbon-Based Materials as Supercapacitor Electrodes. *Chem. Soc. Rev.* **2009**, *38*, 2520−2531.
(24) Ray, A.; Saruhan, B. Application of Ionic Liquids for Batteries and Supercapacitors. *Materials* **2021**, *14*, 2942.
(25) Ahrenberg, M.; Beck, M.; Neise, C.; Keßler, O.; Kragl, U.; Verevkin, S. P.; Schick, C. Vapor Pressure of Ionic Liquids at Low Temperatures from AC-Chip-Calorimetry. *Phys. Chem. Chem. Phys.* **2016**, *18*, 21381−21390.
(26) Zhang, X.; Wang, L.; Peng, J.; Cao, P.; Cai, X.; Li, J.; Zhai, M. A Flexible Ionic Liquid Gelled PVA-Li2SO4 Polymer Electrolyte for Semi-Solid-State Supercapacitors. *Adv. Mater. Interfaces* **2015**, *2*, 1500267.
(27) Yang, K.; Cho, K.; Yoon, D. S.; Kim, S. Bendable solid-state supercapacitors with Au nanoparticle-embedded graphene hydrogel films. *Sci. Rep.* **2017**, *7*, 40163.
(28) Wee, G.; Salim, T.; Lam, Y. M.; Mhaisalkar, S. G.; Srinivasan, M. Printable photo-supercapacitor using single-walled carbon nanotubes. *Energy Environ. Sci.* **2011**, *4*, 413−416.
(29) Hsu, C.-Y.; Chen, H.-W.; Lee, K.-M.; Hu, C.-W.; Ho, K.-C. A Dye-Sensitized Photo-Supercapacitor Based on PProDOT-Et2 Thick Films. *J. Power Sources* **2010**, *195*, 6232−6238.
(30) Xu, J.; Ku, Z.; Zhang, Y.; Chao, D.; Fan, H. J. Integrated Photo-Supercapacitor Based on PEDOT Modified Printable Perovskite Solar Cell. *Adv. Mater. Technol.* **2016**, *1*, No. 1600074.
(31) Zhang, C.; Xu, S.; Cai, D.; Cao, J.; Wang, L.; Han, W. Planar Supercapacitor with High Areal Capacitance Based on Ti3C2/Polypyrrole Composite Film. *Electrochim. Acta* **2020**, *330*, No. 135277.
(32) Liang, J.; Zhu, G.; Lu, Z.; Zhao, P.; Wang, C.; Ma, Y.; Xu, Z.; Wang, Y.; Hu, Y.; Ma, L.; et al. Integrated Perovskite Solar Capacitors with High Energy Conversion Efficiency and Fast Photo-Charging Rate. *J. Mater. Chem. A* **2018**, *6*, 2047−2052.
(33) Liang, J.; Zhu, G.; Wang, C.; Zhao, P.; Wang, Y.; Hu, Y.; Ma, L.; Tie, Z.; Liu, J.; Jin, Z. An All-Inorganic Perovskite Solar Capacitor for Efficient and Stable Spontaneous Photocharging. *Nano Energy* **2018**, *52*, 239−245.
(34) Song, Z.; Wu, J.; Sun, L.; Zhu, T.; Deng, C.; Wang, X.; Li, G.; Du, Y.; Chen, Q.; Sun, W.; et al. Photocapacitor Integrating Perovskite Solar Cell and Symmetrical Supercapacitor Generating a Conversion Storage Efficiency Over 20%. *Nano Energy* **2022**, *100*, No. 107501.
(35) Liu, R.; Wang, J.; Sun, T.; Wang, M.; Wu, C.; Zou, H.; Song, T.; Zhang, X.; Lee, S.-T.; Wang, Z. L.; Sun, B. Silicon Nanowire/Polymer Hybrid Solar Cell-Supercapacitor: A Self-Charging Power

https://doi.org/10.1021/acsomega.3c09812
ACS Omega 2024, 9, 7255−7261

Unit with a Total Efficiency of 10.5%. *Nano Lett.* **2017**, *17*, 4240−4247.
(36) McCloskey, B. D. Expanding the Ragone Plot: Pushing the Limits of Energy Storage. *J. Phys. Chem. Lett.* **2015**, *6*, 3592−3593.

https://doi.org/10.1021/acsomega.3c09812
ACS Omega 2024, 9, 7255−7261